JOURNAL OF CATALYSIS 155, 403–413 (1995)

Olefins by Catalytic Oxidation of Alkanes in Fluidized Bed Reactors[1]

S. S. Bharadwaj and L. D. Schmidt[2]

Department of Chemical Engineering and Materials Science, University of Minnesota, Minneapolis, Minnesota 55455

Received January 6, 1995; revised May 2, 1995

The production of ethylene or syngas from ethane and olefins from propane, *n*-butane, and isobutane in the presence of air or O_2 at atmospheric pressure has been examined over 100 μm α-Al_2O_3 beads coated with noble metals in a static fluidized bed reactor at contact times from 0.05 to 0.2 s. Variations in feed composition, preheating temperature, and flow rate were examined. For ethane on Pt, we observe selectivities to ethylene in excess of 72%, with conversions above 85% at the oxidative dehydrogenation stoichiometry (alkane/O_2 = 2.0) for a 62% single-pass yield which is 5% higher than previously observed on Pt monoliths. On Rh, CO, and H_2 (syngas) production dominates with CO and H_2 selectivities up to 90% at nearly 100% ethane conversion. With propane and *n*-butane on Pt, we observe 55–60% and 65–70% selectivity to olefins, respectively, with >90% conversion for both alkanes. Ethylene and propylene are the major olefin products for both alkanes. Ethylene production dominates at higher temperatures and longer contact times while propylene production is favored at lower temperatures and shorter contact times. With isobutane on Pt, we observe 60–70% olefins with 80% conversion with isobutylene and propylene as the dominant olefins. For all alkanes, C_2H_2 formation was ≤0.8% and C_4H_6 and aromatics were less than 0.05%. Although all experiments were carried out in a regime predicted to be severely coke forming, no carbon buildup was observed on any of the catalysts and the catalysts exhibit no evidence of deactivation over several days. A simple reaction mechanism appears to explain the observed product distributions. Reactions are initiated by oxidative dehydrogenation of the alkane by adsorbed oxygen to form a surface alkyl. On Pt, β-hydrogen and β-alkyl elimination reactions of adsorbed alkyl dominate, which lead to olefins rather than cracking to C_s and H_s. On Rh, Ni, and Pd β-hydrogen elimination is not preferred and cracking to C_s and H_s ultimately leads to syngas production (Rh, Ni) or carbon deposition (Pd).

1. INTRODUCTION

Light alkanes are the preferred feedstocks for producing olefins by thermal pyrolysis. However, thermal dehydrogenation processes for olefin production are highly endothermic and require complex tube furnaces. Excess steam (~50% by volume) is necessary to slow coke formation, and the products contain acetylenes, diolefins, and aromatics in addition to the desired olefins (1).

An alternate route to olefin production is oxidative dehydrogenation of alkanes, which offers the advantages of faster and exothermic oxidation reactions. In earlier investigations of both catalytic (over oxide catalysts such as V_2O_5/SiO_2) and noncatalytic oxidative dehydrogenation (10–21), the conversions at the desired selectivity levels were too low to give acceptable product yields (typically >80% selectivity at <20% conversion). However, in recent investigations in this laboratory, olefin production by catalytic oxidation of light alkanes was studied over Pt- and Rh-coated ceramic foam monoliths at contact times on the order of milliseconds (Huff and Schmidt, (2–4)). Although under the reaction conditions of their study the products predicted at thermodynamic equilibrium were predominantly CH_4, CO, H_2, and solid carbon, olefin selectivities in the range 65–70% at >80% conversion were observed on Pt monoliths for ethane, propane, *n*-butane, and isobutane with no carbon formation. With C_2H_6 on Rh, syngas production dominated, while on Pd heavy carbon deposition rapidly occurred. Huff *et al.* proposed that reactions were initiated by catalytic oxidative dehydrogenation of the alkane by adsorbed O_2 to form a surface alkyl which subsequently underwent β-hydrogen and β-alkyl elimination reactions on Pt to give olefins. On Rh or Pd β-elimination reactions were not preferred, resulting in complete pyrolysis of the adsorbed hydrocarbon to C_s and H_s species which ultimately lead to syngas formation on Rh and coke on Pd.

In this study, we investigate olefin production by catalytic partial oxidation of C_2H_6, C_3H_8, *n*-C_4H_{10}, and *i*-C_4H_{10} on noble metal catalysts in fluidized bed reactors with the aim of identifying conditions for maximizing olefin selectivities, understanding the reaction mechanism, and examining the effect of reactor type and geometry on these reaction systems. Only a few partial oxidation processes in industry today use fluidized bed reactor technology, for example, BP-Sohio's acrylonitrile process by the ammoxidation of propylene (5) and DuPont's *n*-butane to maleic anhydride process in riser reactors (6, 7), both of which use oxide catalysts.

Our experiments are in the turbulent regime and should

[1] This research was supported by NSF Grant CTS-9311295.

[2] To whom correspondence should be addressed.

0021-9517/95 $12.00

TABLE 1

Reactions of Alkanes, Stoichiometric Ratios, and Heats of Reaction

Reaction and products	Ethane		Propane		Butane	
	C_2/O_2	ΔH (kJ/mol)	C_3/O_2	ΔH (kJ/mol)	C_4/O_2	ΔH (kJ/mol)
Total oxidation, $CO_2 + H_2O$	0.286	−1429	0.2	−2043	0.15	−2657
Synthesis gas, $CO + H_2$	1	−137	0.667	−227	0.5	−568
Oxidative dehydrogenation, corresp. olefin + H_2O	2	−105	2	−118	2	−116
Oxidative cracking, lower olefins + H_2O	—	—	—	—	2	−12
Dehydrogenation, corresp. olefin	—	+136	—	+124	—	+126
Cracking						
olefin + CH_4	—	—	—	+83	—	+70
olefin + paraffin	—	—	—	—	—	+92

give a good simulation of large fluidized beds with high heat transfer characteristics. We recently reported highly selective syngas formation from CH_4 by catalytic partial oxidation in fluidized bed reactors on Rh and Ni catalysts (Bharadwaj and Schmidt (8)) and this work is an extension from CH_4 to higher alkanes. We will show that in the fluidized bed we achieve higher olefin selectivities and alkane conversions than on monoliths to give ~5% higher single-pass olefin yields.

2. REACTIONS

The stoichiometric fuel/O_2 ratios and heats of reaction for alkane oxidation reactions are listed in Table 1. Reactions of *n*-butane are listed below as an example.

A. Exothermic Reactions

In the presence of O_2, hydrocarbons can be totally or partially oxidized depending on the feed composition (fuel/O_2). In increasing order of the fuel/O_2 ratio they can either be totally oxidized [1], partially oxidized to syngas [2], or oxidatively dehydrogenated to the corresponding olefin [3]. Butane can also be oxidatively cracked [4].

$$C_4H_{10} + \frac{13}{2}O_2 \rightarrow 4\,CO_2 + 5\,H_2O \quad \text{combustion} \quad [1]$$

$$C_4H_{10} + 2\,O_2 \rightarrow 4\,CO + 5\,H_2 \quad \text{syngas} \quad [2]$$

$$C_4H_{10} + \frac{1}{2}O_2 \rightarrow C_4H_8 + H_2O \quad \text{olefins} \quad [3]$$

$$C_4H_{10} + \frac{1}{2}O_2 \rightarrow 2\,C_2H_4 + H_2O \quad \text{cracking} \quad [4]$$

B. Endothermic Reactions

Besides oxidation reactions, dehydrogenation [5] and cracking [6, 7] reactions can also take place at high temperatures.

$$C_4H_{10} \rightarrow C_4H_8 + H_2 \quad \text{dehydrogenation} \quad [5]$$

$$C_4H_{10} \rightarrow CH_4 + C_3H_6 \quad \text{cracking} \quad [6]$$

$$C_4H_{10} \rightarrow C_2H_4 + C_2H_6 \quad \text{cracking} \quad [7]$$

C. Carbon-Forming Reactions

The product species can also react to form solid carbon (C_s) via olefin cracking [8], CO disproportionation (Boudouard reaction) [9], and reverse steam reforming of carbon [10].

$$\text{olefin} \rightarrow C_s + H_2 \quad \text{olefin cracking} \quad [8]$$

$$2\,CO \rightarrow C_s + CO_2 \quad \text{CO disproportionation} \quad [9]$$

$$CO + H_2 \rightarrow C_s + H_2O \quad \text{reverse steam reforming of } C_s \quad [10]$$

3. EQUILIBRIUM

Thermodynamic equilibrium calculations by Huff and Schmidt (2, 3, 4) predict solid graphite to be the major product at all temperatures for fuel/O_2 compositions richer than that for syngas, and at lower temperatures graphite is stable at even leaner fuel compositions. Since no carbon deposition was observed in their experiments, equilibrium calculations were also performed where solid carbon formation was not allowed by allowing its activity to be less than unity. Even with this limitation, thermodynamics predicts only CH_4, CO, and H_2 as the major products with negligible olefin formation. Evaluation of experimental equilibrium constants suggested that on Pt, the olefin cracking reaction [8] must not reach equilibrium and that the CO_2 and H_2O partial pressures were high enough to suppress graphite formation caused by alkane and olefin cracking by CO_2 and steam reforming of C_s (Eqs. [9] and [10]).

4. EXPERIMENTS

Apparatus and Procedure

The reactors used were essentially identical to those described previously for synthesis gas production from methane (8). The reactors were quartz tubes (1.9–3.2 cm diameter with 8–12 cm bed height) with expanded sections at the top for catalyst disengagement. A porous 40 μm quartz frit served as a gas distributor and support plate. The entire reactor was wound with high-temperature heating tape and insulated. Gas flow into the reactor was controlled by mass flow controllers. The feed flow rates ranged from 0.5 to 2.0 slpm total flow, corresponding to 1.0 to 4 cm/s superficial velocity (i.e., the velocity of the feed gases upstream from the catalyst) at room temperature and atmospheric pressure. The product gases were sampled just before the expansion with a gas tight syringe through a septum-covered sample port or through heated lines leading to the GC. A coarse 175 μm pyrex frit was loosely fitted in the disengagement section to prevent blowout of fines.

The GC analysis was performed using a single Hayesep DB packed column with temperature programming. For quantitative determination of concentrations, standards were used for all species except H_2O, which was obtained most reliably from an oxygen atom balance. The mole number change due to reaction was determined by an atomic balance on nitrogen, and 15–25% N_2 was added for oxygen experiments. The product gas carbon atom and hydrogen atom balances typically closed to within $\pm 2\%$.

Temperatures were monitored using two thermocouples, one before the quartz frit and one in the catalyst bed. In order to determine the heat input through the heating tape, the feed gas temperature and the bed temperature were measured for a fixed power input without reaction by flowing air through the reactor.

All experiments for the results reported here were carried out in a 3.2 cm diameter reactor using 15–20 g of catalyst. The unfluidized bed depth was ~2 cm and the expansion was approximately a factor of two, which corresponded to a solid fraciton of ~0.25. Depending on the total flow rate and bed expansion, the contact times at reaction temperatures (~850°C) and nearly complete conversion were between 0.05 and 0.3 s.

Catalyst Preparation

All catalysts were prepared by deposition and decomposition of the respective salts on low surface area, attrition-resistant α-Al_2O_3 supports. The alumina spheres, specially prepared for fluidization applications, were supplied by Norton Chemical Process Products Corporation and had a particle size range of 80–100 μm, a surface area ~0.3 m^2/g, and an internal pore volume ~0.2 cm^3/g. The bulk density of the fixed bed was ~1.1 g/cm^3 (9). For metal deposition, the alumina was stirred in a heated salt solution of known concentration until most of the water evaporated. The wet spheres were dried and then calcined for 2–3 h at the appropriate temperature to decompose the salt. Catalysts with loadings of 0.25–2.0 wt% were prepared.

Light-off

Light-off was achieved by preheating the catalyst bed to 300–350°C in air or N_2 and then introducing the fuel/O_2 mixture. At light-off the temperature rose rapidly and attained steady state (700–800°C) within a few minutes, which was a function of the overall heat generation rate due to chemical reaction, the heat input through the heating tape, the energy carried by the product gases, and the rate of energy loss from the reactor by conduction, convection, and radiation.

Throughout these experiments we detected no changes in activity or selectivities from 10 min after ignition to at least 5 h of operation for fixed inlet conditions. Identical steady state temperatures and product compositions could be repeated on returning to the original conditions after several changes in feed conditions and flow rates. Positioning of the thermocouple at different locations in the catalyst bed indicated that the bed was isothermal within ±25°C and no hot spots were detected which indicates good solids mixing in the fluidized bed.

The autothermal temperatures (no external heating) were typically between 550–850°C for room temperature feed gases, depending on the stoichiometric composition of the fuel/O_2 mixture, N_2 diluent, amount of catalyst in the reactor, flow rate, and the reactor used. With richer feeds, less exothermal reactions take place, giving lower autothermal temperatures. Moreover, in a fluidized bed the high-heat transfer coefficients and solids backmixing promote heat losses. In most experiments, the reactor was heated externally to raise the temperature of the reaction mixture above 750°C to achieve better yields. The problem of heat losses is typical in small-scale equipment. A large-scale reactor, on the other hand, is expected to operate at higher autothermal temperatures, eliminating the need for additional heat input but also making it difficult to adjust reactor temperature.

5. RESULTS

We examined the effects of feed composition, reaction temperatures, and flow rates for all the C_1–C_4 alkanes on Pt catalysts. Experiments were performed using both air and almost-pure O_2 (15% N_2 diluent). We also looked at several different catalysts for C_2H_6; Pt, Rh, Ni, Pd, Pt–Au (all supported on α-Al_2O_3), and Pt/ZrO_2. All results are shown here as selectivities calculated on a carbon or hydrogen atom basis.

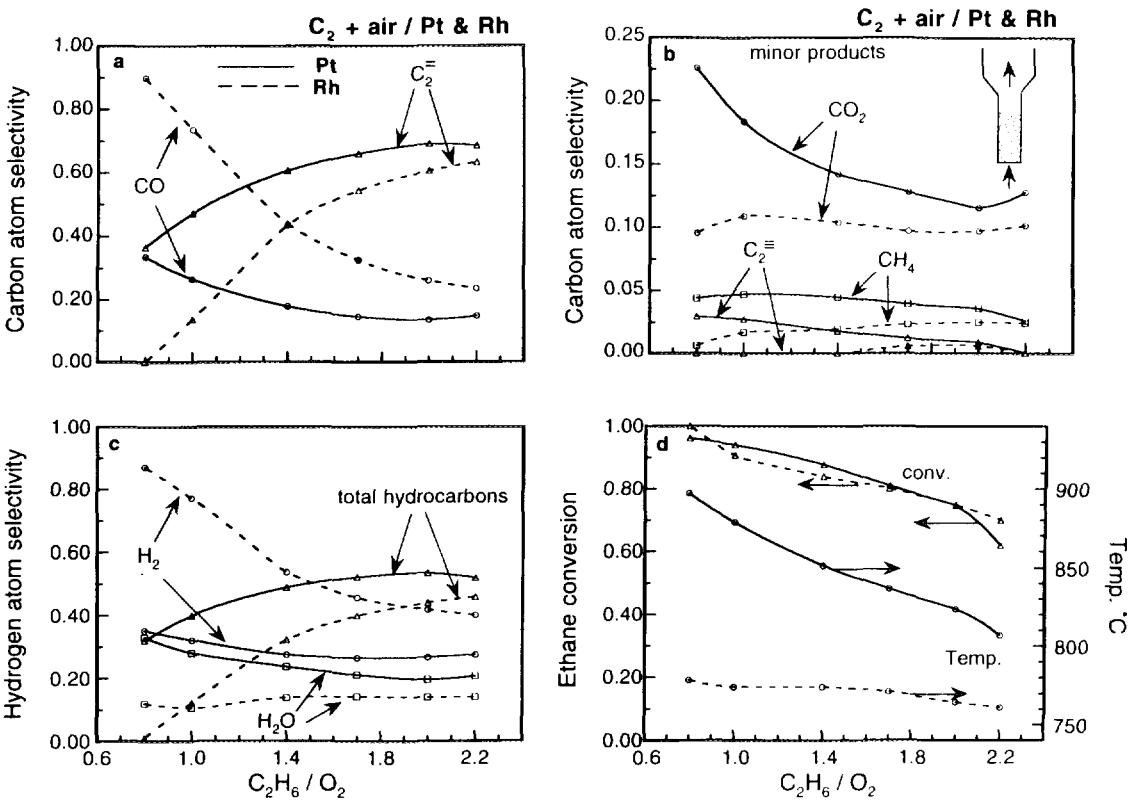

FIG. 1. Plots of effect of feed composition on carbon and hydrogen atom selectivities, ethane conversions, and bed temperatures (°C) for ethane oxidation on Pt and Rh with air at a total flow rate of 1.5 slpm. Solid lines represent Pt and dotted lines represent Rh.

Ethane

Air on Pt and Rh. Figure 1 shows the fractional carbon and hydrogen atom selectivities, conversions, and temperatures for feed mixtures of ethane and air on Pt and Rh as a function of the feed composition. Identical conditions (flow, heat input, and composition) in the same reactor allowed observations for Pt and Rh to be compared directly. The feed composition was varied maintaining constant total flow rate (1.5 slpm) and heat input. To facilitate comparison with O_2 experiments shown later, the feed composition is represented by the C_2H_6/O_2 ratio rather than the percentage of ethane in air. The C_2H_6/O_2 ratio for syngas is 1.0 and that for oxidative dehydrogenation is 2.0. Experiments were performed in the range 0.8 to 2.2 and the O_2 conversion was complete at all compositions.

As seen in Fig. 1, at $C_2H_6/O_2 = 0.8$, the CO and H_2 selectivities on Rh are ~90% with complete ethane conversion and no ethylene formation. However on Pt at the same composition, the CO and H_2 selectivities are lower (~35%) while ethylene is produced with 37% selectivity with 96% ethane conversion. This is surprising since, as noted above, thermodynamics predicts CO, H_2, CH_4, and graphite with no other significant byproducts. As the C_2H_6/O_2 ratio is increased, the ethylene selectivity increases on both metals. At the oxidative dehydrogenation stoichiometry (2.0), the ethylene selectivity on Pt reaches as high as 70% while that on Rh reaches 60%. The conversion on both is ~75%, which corresponds to ethylene yields of 52.5% on Pt and of 45% on Rh. Beyond $C_2H_6/O_2 = 2$, there is no significant gain in selectivity and the conversion drops.

Oxygen on Pt. In Figs. 2a and 2b, we show the carbon selectivities, conversion, and bed temperature for ethane oxidation in O_2 on Pt as a function of feed composition. The feed composition was varied maintaining 15% N_2 in the feed at a total flow rate of 1.5 slpm. The observed trends are similar to those for the air experiments. In the presence of reduced N_2 diluent, the reaction temperatures are higher. At $C_2H_6/O_2 = 2$, the ethylene selectivity and ethane conversion are 72% and 70%, respectively, giving a yield of 50.4%.

The conversion can be improved by increasing the reaction temperature as shown in Figs. 2c and 2d. The reaction temperature was varied by varying the heat input at fixed flow rate (1.5 slpm) and composition ($C_2H_6/O_2 = 2$). With an increase in the reaction temperature to 870°C, the ethane conversion exceeds 90% while the ethylene selectivity drops to 67%. However, yields in excess of 60% are ob-

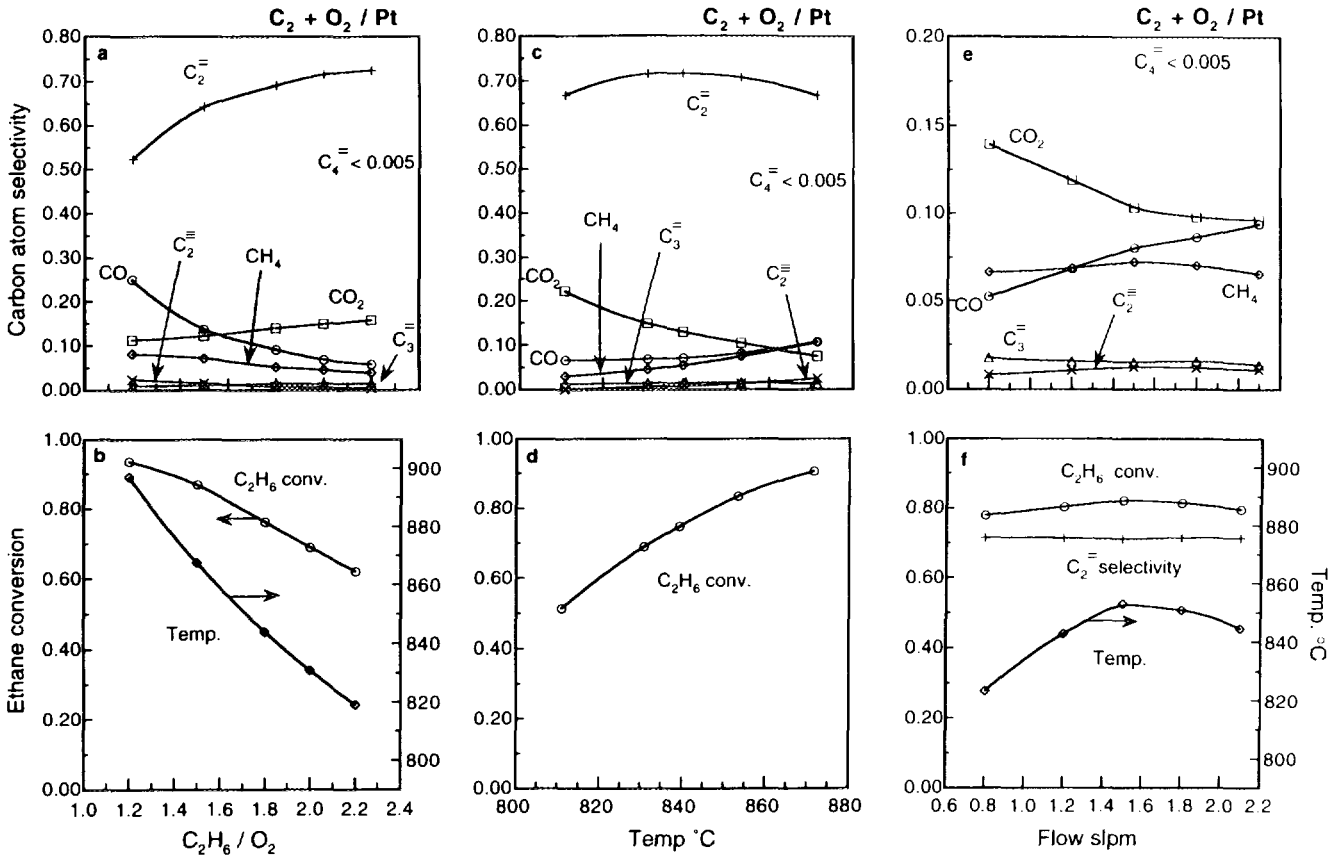

FIG. 2. Plots of ethane oxidation on Pt using O_2 (15% N_2 diluent). Panels a and b show the effect of feed composition on carbon atom selectivities, ethane conversion, and bed temperature at a total flow rate of 1.5 slpm. Panels c and d show the effect of temperature on carbon atom selectivities and ethane conversion at a total flow rate of 1.5 slpm and C_2H_6/O_2 = 2.0. Panels e and f show the effect of flow rate on carbon atom selectivities, ethane conversion and bed temperature at C_2H_6/O_2 = 2.0.

tained (86% conversion with 70% selectivity or 90% conversion with 67% selectivity), which are considerably higher than those obtained in thermal pyrolysis in a single pass (typically 48% (1)).

Figures 2e and 2f illustrate the effect of flow rate on the selectivities, conversions, and temperatures at C_2H_6/O_2 = 2 for fixed heat input. It can be seen that a threefold variation in superficial contact time produces no significant change in the ethylene selectivity (~70%) and ethane conversion (80%).

Other catalysts: Ni, Pd, Pt–Au, Pt/ZrO₂. We also examined Ni and Pd catalysts on the same α-Al_2O_3 support. Figures 3a and 3b show the effect of ethane feed composition on carbon selectivities, conversion, and temperature for ethane oxidation on Ni in air. We see that Ni is very similar to Rh with high CO and H_2 selectivities near the syngas stoichiometry and ethylene selectivity up to 60% at the oxidative dehydrogenation stoichiometry. We also note that both Ni and Rh were found to be extremely good catalysts for producing syngas from CH_4 (Bharadwaj and Schmidt (8)). With Pd, the catalyst rapidly coked after light-off just as was observed on monoliths and the reaction shut off in less than 10 min.

We also examined Pt–Au catalysts with the aim of reducing the hydrogenolysis activity by reducing Pt ensemble size by Au addition. However, results obtained with Pt–Au were very similar to those for Pt, suggesting that the hydrogenolysis activity was low. With Pt/ZrO_2, slightly higher conversions and lower selectivities to ethylene were observed than with Pt/Al_2O_3, just as on monoliths.

Oxygen on Al_2O_3 only. We also performed experiments with pure Al_2O_3 to study the activity of the support. With Al_2O_3, unlike Pt and Rh, light-off is very difficult and gradual, and a much higher heat input is required to achieve high temperatures for acceptable yields. Figures 3c and 3d show the selectivities, conversions, and temperatures for ethane oxidation with O_2 on Al_2O_3 as a function of the feed composition.

We note that these results may be compared with those shown in Figs. 2c and 2d for ethane oxidation on Pt with

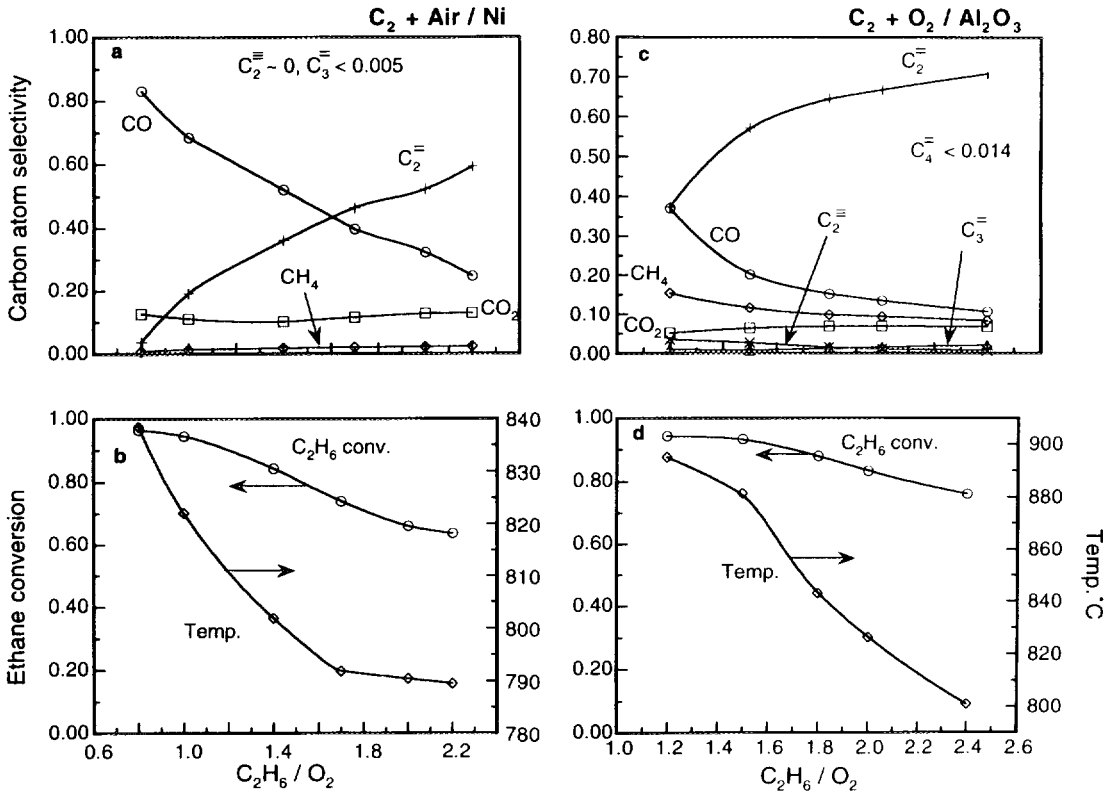

FIG. 3. Plots of ethane oxidation on Ni and α-Al_2O_3. Panels a and b show the effect of feed composition on carbon atom selectivities, ethane conversion, and bed temperature for ethane oxidation on Ni with air at a total flow rate of 1.5 slpm. Panels c and d show the effect of feed composition on carbon atom selectivities, ethane conversion, and bed temperature for ethane oxidation on α-Al_2O_3 with O_2 (15% N_2 diluent) at a total flow rate of 1.5 slpm.

O_2. However, a much higher heat input was necessary for the Al_2O_3 experiments, suggesting that the role of homogeneous reactions is probably higher and surface-assisted homogeneous reactions may be playing an important role. More CO versus CO_2 is obtained on Al_2O_3 than on Pt, which explains the need for higher heat input because CO_2 formation is much more exothermic. Also CH_4 production is significantly greater on Al_2O_3 and is >10% compared to <5% on Pt, suggesting more cracking activity. However, we do not observe any carbon deposition on the Al_2O_3 particles even at extremely rich fuel compositions ($C_2H_6/O_2 \sim 3$).

At $C_2H_6/O_2 = 2$, the ethylene selectivity and ethane conversion on Al_2O_3 are 67% and 83%, respectively. Optimum yields are obtained at temperatures near ~810°C. Beyond $C_2H_6/O_2 = 2$, although the ethylene selectivity continues to increase, higher heat input is necessary to sustain high temperatures for high conversion. At $C_2H_6/O_2 = 3$, the ethylene selectivity is 82% and the conversion is 72% (with even higher heat input).

Propane and n-Butane on Pt

We examined propane and *n*-butane oxidation on 0.5 wt% Pt/Al_2O_3 using both air and O_2. Since the results with air and O_2 are quite similar (the only difference being the higher temperatures obtained with O_2), only the O_2 data are shown. Ethylene and propylene were the major olefins obtained from both alkanes and the product distributions had similar features suggesting that the mechanism for olefin formation was the same for both hydrocarbons. Figures 4a–4f, show selectivity and conversion data for *n*-butane. Data for propane are not shown because trends for propane can be deduced from *n*-butane data.

Figures 4a and 4b show the selectivities, conversion, and temperature for *n*-butane oxidation with O_2 on Pt as a function of the feed n-C_4H_{10}/O_2 ratio. At low feed compositions (n-$C_4H_{10}/O_2 = 1.3$), butane conversion is nearly complete with a total olefin selectivity of ~59% ($C_2^=:C_3^=:1\text{-}C_4^= = 46:11:2$). As the feed composition is increased, the temperatures and conversions decrease with the total olefin selectivity rising to 66% ($C_2^=:C_3^=:1\text{-}C_4^= = 36:27:3$) at the oxidative dehydrogenation stoichiometry (n-$C_4H_{10}/O_2 = 2.0$). We note that increase in feed composition causes the ethylene selectivity to decrease while the propylene selectivity increases. Also the ratio of the C_2H_4 and CH_4 carbon atom selectivities is ~2 over the entire compo-

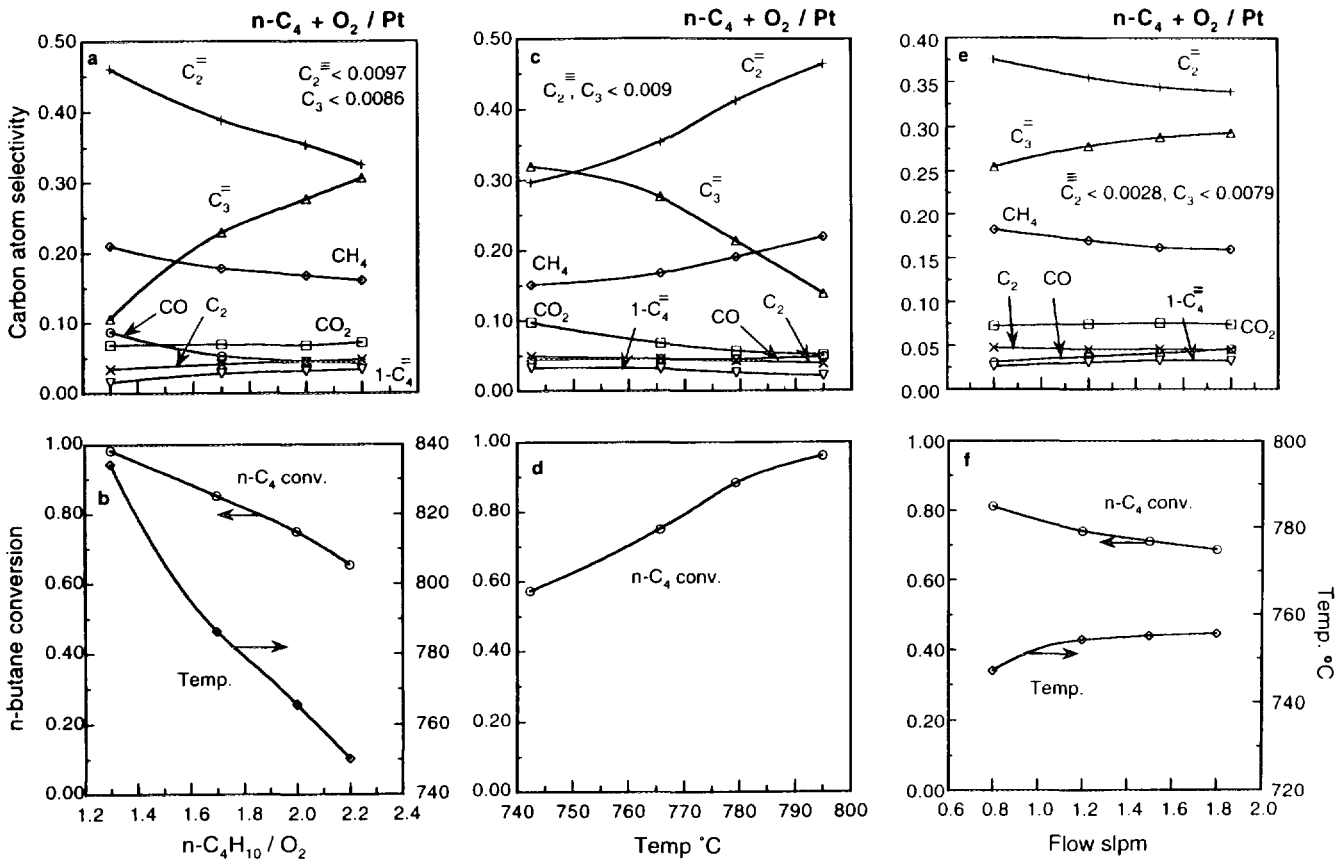

FIG. 4. Plots of *n*-butane oxidation on Pt using O_2 (25% N_2 diluent). Panels a and b show the effect of feed composition on carbon atom selectivities, *n*-butane conversion, and bed temperature at a total flow rate of 1.5 slpm. Panels c and d show the effect of temperature on carbon atom selectivities and *n*-butane conversion at a total flow rate of 1.5 slpm and $n\text{-}C_4H_{10}/O_2 = 2.0$. Panels e and f show the effect of flow rate on carbon atom selectivities, *n*-butane conversion, and bed temperature at $n\text{-}C_4H_{10}/O_2 = 2.0$.

sition range, suggesting that the process involves cracking of propylene into C_2H_4 and CH_4.

The effect of temperature on the selectivities and conversions at $n\text{-}C_4H_{10}/O_2 = 2.0$ is shown in Figs. 4c and 4d. We can see that by increasing the temperature the conversion, which is 60% at 745°C, can be increased to almost 95% at ~800°C. The total olefin selectivity drops slightly from 65 to 61%. Here we see an opposite trend in the olefin selectivity distribution. With increasing temperature, more ethylene and CH_4 and less propylene are produced.

Figures 4e and 4f show the effects of varying the contact time at $n\text{-}C_4H_{10}/O_2 = 2.0$ for fixed heat input. With increasing flow rate, there is a slight increase in the total olefin selectivity along with a small drop in conversion. As expected, we see that propylene increases while ethylene and CH_4 both decrease in the same manner as before. The survival of propylene with decreasing contact time strongly suggests that the mechanism involves cracking of propylene.

Results with propane were very similar. In summary, both propane and *n*-butane can be converted to olefins with 60–70% selectivity and 90%+ conversion. Ethylene production dominates at high temperatures and long contact times while propylene production is maximized at lower temperatures and short contact times. We note here that very low amounts of butenes are produced with *n*-butane, which cracks readily to give lower olefins.

Isobutane on Pt

Isobutylene is chiefly used to produce methyl tertiary-butyl ether (MTBE). In current commercial processes, thermal dehydrogenation of isobutane gives isobutylene yields up to 20% (1). However, the process is highly endothermic and byproducts such as diolefins and aromatics are also obtained. Although good selectivities to isobutylene (~80%) have been achieved with catalytic oxidative dehydrogenation on a number of oxide catalysts, the low conversions (<10%) make the yields unacceptable (21).

In our fluidized bed experiments we can achieve isobu-

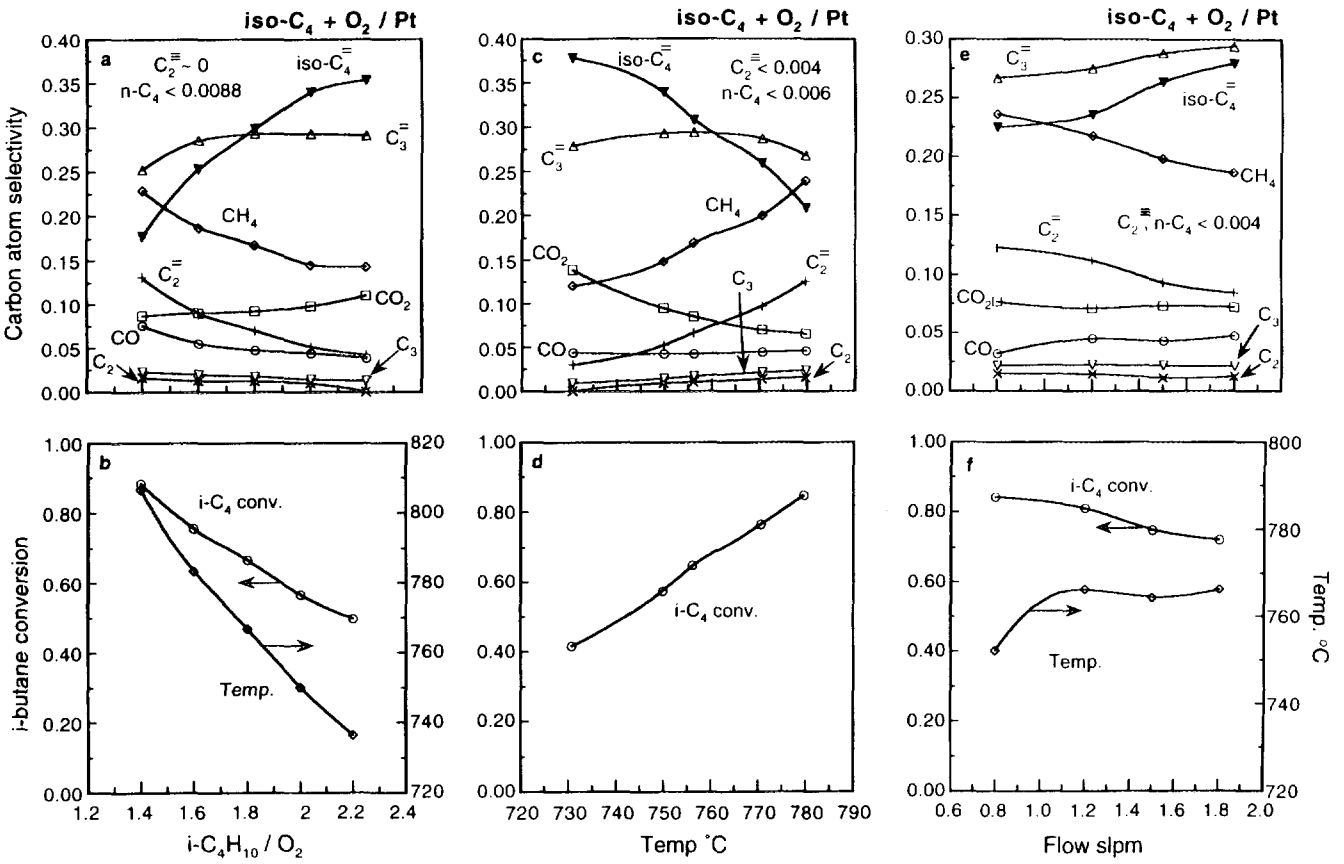

FIG. 5. Plots of iso-butane oxidation on Pt using O_2 (25% N_2 diluent). Panels a and b show the effect of feed composition on carbon atom selectivities, iso-butane conversion, and bed temperature at a total flow rate of 1.5 slpm. Panels c and d show the effect of temperature on carbon atom selectivities and iso-butane conversion at a total flow rate of 1.5 slpm and i-C_4H_{10}/O_2 = 2.0. Panels e and f show the effect of flow rate on carbon atom selectivities, iso-butane conversion, and bed temperature at i-C_4H_{10}/O_2 = 2.0.

tane conversions in excess of 80% with total olefin selectivities between 60 and 70%. Figures 5a and 5b show the selectivities, conversion, and temperature for isobutane oxidation with O_2 on Pt as a function of the feed composition at fixed flow rate and heat input. At i-C_4H_{10}/O_2 = 1.4, the conversion is 90% and the total olefin selectivity is 55% (i-$C_4^=$: $C_3^=$: $C_2^=$ = 17.5 : 25 : 12.5). As the feed composition is increased to i-C_4H_{10}/O_2 = 2.0, the total olefin selectivity increases to 68.6% (i-$C_4^=$: $C_3^=$: $C_2^=$ = 34 : 29.5 : 5.1) while the conversion drops to 56%. The olefin distributions show that as the composition approaches that for oxidative dehydrogenation, isobutylene and propylene selectivities increase while the ethylene and CH_4 selectivities decrease.

Figures 5c and 5d show the effect of temperature on the selectivities and conversions at i-C_4H_{10}/O_2 = 2.0. An increase in temperature from 730 to 780°C is accompanied by a decrease in total olefin selectivity from 69 to 60% while the conversion increases from 42 to 86%. Also with increasing temperature more ethylene and CH_4 and less isobutylene are produced. The propylene selectivity does not vary much with temperature.

From Figures 5a–5d we see that isobutylene production is maximized at high alkane compositions (near i-C_4H_{10}/O_2 = 2.0) and lower temperatures. However, at low temperatures, conversions are lower (<60%). To increase conversion we need to increase the temperature which decreases isobutylene selectivity. This decrease might be prevented if the contact time were reduced. Figures 5e and 5f show the results of flow rate variation at i-C_4H_{10}/O_2 = 2.0 for a fixed heat input. As expected, with increasing flow rates we observe an increase in isobutylene and propylene selectivities with a decrease in ethylene and CH_4. The conversion drops slightly.

6. DISCUSSION

Comparison with Monoliths

In the fluidized bed we observe 6–8% higher olefin selectivities at comparable conversion levels to give olefin yields almost 5% higher than those observed on Pt monoliths (Huff *et al.* (2–4)). The general trends in selectivities and conversions in the fluidized bed with variations in process

parameters are otherwise very similar to those obtained for monoliths. However, contact times in the fluidized bed (50–200 ms) are significantly higher than on monoliths (5–10 ms). Also, the temperatures are slightly lower (850°C in the fluidized bed and 1000°C on the monolith). Similar product distributions, however, suggest that reaction steps are the same in both reactors.

The fluidized bed is certainly well mixed with respect to the catalyst. The solids backmixing efficiently carries heat back upstream to maintain isothermal conditions throughout the reactor. A monolith on the other hand relies exclusively on solid conduction and radiation to carry heat upstream to minimize temperature gradients.

However, in the fluidized bed the gases are probably close to plug-flow just as in monolith reactors. We believe that almost all the O_2 is consumed close to the distributor region. Flow past the small 100-μm particles at high velocities (22.5 cm/s at reaction conditions) results in thin boundary layers and enhanced mass transfer rates which result in rapid and complete O_2 consumption. If the region containing O_2 is assumed to be 2 mm thick, the contact time at reaction conditions is 8.9 ms, which is of the same order of magnitude as on monoliths (5–10 ms). Therefore, once all the O_2 has been reacted, the olefins leave the reactor without reacting further. Higher gas backmixing would lead to olefin + O_2 reactions and selectivity loss because olefins are more reactive than alkanes, and at lower flow rates we do see selectivity losses. This explanation accounts for complete conversion of the alkane, survival of the olefin, and even better performance than monoliths at apparently longer contact times in a more mixed reactor configuration.

Comparison of Catalysts

As described above, we examined several different catalysts with ethane. Pt was found to be the best catalyst for ethylene, Pt–Au gave very similar results, while Rh and Ni were extremely good syngas catalysts near the syngas stoichiometry (C_2H_6/O_2 = 1.0) and produced C_2H_4 with selectivities up to 60% near the oxidative dehydrogenation stoichiometry. On Pd, reactions eventually go to chemical equilibrium, which produces carbon. Pt/ZrO_2 gives slightly better conversions and lower selectivities than Pt/Al_2O_3.

Although α-Al_2O_3 did give appreciable ethylene yields, it was difficult to ignite, and high heat input was required to maintain the reactor at reaction conditions. Also, trace amounts of many product peaks were observed. We note here that it has not been possible to do this experiment on a monolith, because at the shorter contact times in the absence of solids backmixing to efficiently transfer heat, α-Al_2O_3 is almost impossible to ignite.

Recently, we have examined high-temperature (800–1000°C) oxidation of ethane on Ag/Al_2O_3, both in fluidized beds and on monoliths. We observe highly selective ethylene formation from ethane although alkanes are less reactive on Ag than on Pt. This will be the subject of a later publication.

Mechanism

We believe that reactions on the noble metal catalysts are predominantly heterogeneous and the reaction mechanism is essentially the same as that proposed by Huff and Schmidt for the oxidative dehydrogenation of ethane (2) and oxidative cracking of propane and butanes (3, 4). This mechanism satisfactorily explains the observed results of (1) high olefin yields, (2) no carbon deposition or deactivation as predicted by thermodynamic equilibrium, (3) similar product distributions from propane and butane, (4) high isobutylene yields from isobutane, and (5) a difference in reaction path on Pt, Rh, Ni, and Pd.

According to the mechanism, the catalyst surface enhances alkane dissociation by hydrogen abstraction with adsorbed oxygen (oxidative dehydrogenation) leading to the adsorbed alkyl. Adsorbed alkyls cannot easily react with gas-phase species because their reactive ends are bound to the surface. Efficient energy exchange at the surface then allows unimolecular reactions of adsorbed alkyls such as β-hydrogen and β-alkyl elimination to dominate and yield the simple mix of products observed. The surface also accomplishes a reduction of bimolecular reaction steps which lead to the formation of diolefins, polymers, and aromatics as in homogeneous thermal pyrolysis.

Ethane. Ethylene is produced by β-hydrogen elimination of the adsorbed ethyl. α-Hydrogen elimination leads to C_s and H_s species giving CH_4, CO, CO_2, and H_2O on Pt, Rh, and Ni or coke on Pd.

Propane and n-butane. For propane and *n*-butane, β-alkyl elimination is favored over β-hydrogen elimination. When the primary carbon atom adsorbs, β-methyl elimination of *n*-propyl and β-ethyl elimination of *n*-butyl lead to C_2H_4. Adsorption of the secondary carbon atom results in C_3H_6 from both alkanes (via β-hydrogen elimination of adsorbed isopropyl and β-methyl elimination of adsorbed 2-butyl). At higher temperatures, more C_2H_4 is formed, which is explained by the higher activation energy for C_2H_4 formation. Increasing the flow rates decreases the contact time and allows formation of more C_3H_6. Just as with ethane, α-hydrogen elimination eventually leads to CH_4, CO, CO_2, and H_2O.

Isobutane. With isobutane, adsorption of the tertiary carbon atom followed by β-hydrogen elimination leads to isobutylene. Adsorption of a primary carbon leads to C_3H_6 and CH_4 via elimination of a β-methyl. CO, CO_2, CH_4, and H_2O are produced either by α-methyl elimination from a tertiary butyl or α-hydrogen elimination from a primary isobutyl.

Role of Homogeneous Reactions

Although our results appear to be explained well by a heterogeneous mechanism we are not certain whether homogeneous reactions can be neglected. For the noble metal catalysts the simple mixture of products obtained suggests that heterogeneous reactions dominate and homogeneous reactions play a minor role.

As discussed by Huff and Schmidt, a simple pyrolysis mechanism cannot predict the high selectivity to olefins. C_2H_4 survives although it is more reactive than C_2H_6 and should crack and oxidize easily. Feed mixtures in our experiments are far outside the flammability regime, which reduces the possibility of homogeneous oxidation reactions. Also, the 100 μm catalyst particles provide a large surface area to scavenge free radical chain propagators.

The differences in product distributions on different metals (Pt (olefins), Rh and Ni (syngas), and Pd (coke)) further suggest that heterogeneous reactions dominate. Also no carbon deposition was observed even at extremely rich compositions on Pt, Rh, Ag, and Al_2O_3 without any steam input. Carbon deposition was observed with Ni at very rich feed compositions, while Pd coked very rapidly over a wide range of feed compositions.

We believe that almost all O_2 is consumed in the distributor region (within 1 mm of the quartz frit). The contribution of homogeneous reactions would depend strongly on the bubble fraction in the distributor region. The flow in that region is approximately plug-flow in the form of laminar jets, implying a low bubble fraction. Therefore contributions of homogeneous reactions should be low. Homogeneous reactions due to flames in the laminar jets are unlikely because the feed mixture is far outside flammability limits. Also catalyst particles are entrained in the jet which consumes all the O_2 because of the high rates of mass transfer from the gas phase to the catalyst surface.

The role of homogeneous reactions is probably higher in the case of the Al_2O_3 experiments where surface assisted homogeneous reactions may be playing an important role. This is because much higher heat input was required to sustain reactions and trace amounts of many peaks were detected for comparable residence times.

Carbon Formation

Carbon formation takes place either by olefin cracking, CO disproportionation or reverse-steam reforming of carbon as shown before in reactions [8] to [10]. Continued formation of even traces of solid carbon on the catalyst will completely shut the reaction off very quickly. In our experiments, we do not see evidence of carbon buildup on Pt or Rh at steady state. This of course does not imply that there is no carbon on the catalysts but that a true steady state is attained where carbon is gasified at exactly the same rate at which it is deposited. In fact, sometimes at very rich feed compositions (fuel/O_2 > 2.1) we observed that the few catalyst particles that accumulated in the expansion zone were black. However, when these were shaken back into the reactor they were regenerated so that we did not see any black particles in the gray Pt catalyst at the end of the experiment or any deactivation over a period of >10 h of operation.

Calculations of the experimental equilibrium constants (ratios of partial pressures given by equilibrium equations) for reactions [8] to [10] show that on Pt and Rh olefin cracking reactions must not reach equilibrium and that the CO_2 and H_2O partial pressures are high enough to suppress graphite formation by CO disproportionation and reverse steam reforming. On Pd, equilibrium in all reactions leads to heavy carbon buildup. Ni is intermediate between Pt and Pd because we did see some carbon formation on the reactor walls during operation. However, the rates were very slow and the catalyst did not deactivate over a period of 4 h. α-Al_2O_3 did not coke even at fuel/O_2 ratios >3.5. Also, the particles that accumulated in the expansion zone were clean and white.

We note that it is possible to operate at richer fuel compositions without coking in a fluidized bed than on a monolith. This is probably because solids mixing in the fluidized bed aids in preventing carbon buildup, unlike a monolith where a carbon front propagates from the front to the back, eventually deactivating the monolith.

7. CONCLUSIONS

We have shown that C_2 to C_4 alkanes can be converted to olefins in very high yields (>70% selectivity at >85% conversion) by catalytic oxidation in fluidized bed reactors on Pt catalysts at contact times of 50–200 ms and temperatures between 800 and 850°C. We believe that the reactions are predominantly heterogeneous on the noble metals and the mechanism involves alkane adsorption by oxidative H abstraction followed by β-hydrogen or β-alkyl elimination to give olefins. α-Hydrogen elimination reactions of the adsorbed alkyl lead to syngas formation on Rh and Ni, and to coke formation on Pd.

Since the fluidized bed reactor was operated close to the turbulent mode, these results should simulate the behavior of a large-scale reactor operating in the turbulent regime fairly closely, allowing straightforward scale-up. The relatively short contact times would result in reactor sizes at least an order of magnitude smaller than current commercial thermal pyrolysis furnaces. The high selectivities, autothermal operation, and absence of carbon formation in fluidized beds provide an energy efficient alternate route to synthesize olefins from alkanes.

REFERENCES

1. "Pyrolysis: Theory and Industrial Practice" (L. F. Albright, B. L. Crynes, and W. H. Corcoran, Eds.). Academic Press, New York, 1983.
2. Huff, M., and Schmidt, L. D., *J. Phys. Chem.* **97,** 11815–11822 (1993).
3. Huff, M., and Schmidt, L. D., *J. Catal.* **149,** 127–141 (1994).
4. Huff, M., and Schmidt, L. D., *J. Catal.*, in press.
5. Satterfield, C. N., "Heterogeneous Catalysis in Industrial Practice." McGraw Hill, New York, 1991.
6. Contractor, R. M., and Sleight, A. W., *Catal. Today* **1,** 587–607 (1987).
7. Contractor, R. M., and Sleight, A. W., *Catal. Today* **3,** 175–184 (1988).
8. Bharadwaj, S. S., and Schmidt, L. D., *J. Catal.* **146,** 11–21 (1994).
9. Norton Chemical Process Products Corporation, Akron, Ohio.
10. Le Bars, J., Vedrine, J. C., Auroux, A., *Appl. Catal. A* **88,** 179–195 (1992).
11. Morales, E., and Lunsford, J. H., *J. Catal.* **118,** 255–265 (1989).
12. Erdohelyi, A., and Solymosi, F., *J. Catal.* **129,** 497–510 (1991).
13. Erdohelyi, A., and Solymosi, F., *J. Catal.* **123,** 31–42 (1990).
14. Michalakos, P. M., Kung, M. C., Jahan, I., and Kung, H. H., *J. Catal.* **140,** 226 (1993).
15. Burch, R., and Crabb, E. M., *Appl. Catal.* **97,** 49–65 (1993).
16. Burch, R., and Crabb, E. M., *Appl. Catal. A* **100,** 111 (1993).
17. Seshan, K., Swaan, H. M., Smits, R. H. H., van Omens, J. G., and Ross, J. R. H., *in* "New Developments in Selective Oxidation" (G. Centi and F. Trifiro, Eds.), pp. 505–512. Elsevier, Amsterdam, 1990.
18. Kung, M., Nguyen, K., Patel, D., and Kung, H., *in* "Catalysis of Organic Reactions" (D. W. Blackburn, Ed.), p. 289. Dekker, New York, 1990.
19. Owens, L., and Kung, H. H., *J. Catal.* **144,** 202 (1993).
20. Armendariz, H., Aguilar-Rios, G., Salas, P., Valenzuela, M. A., Schifter, I., Arriola, H., and Nava, N., *Appl. Catal. A* **92,** 29 (1992).
21. Takita, Y., Kurosaki, K., Mizuhara, Y., and Ishihara, T., *Chem. Lett.* **2,** 335–338 (1993).